

## Article

# Scale Model Experiments and Simulations to Investigate the Effect of Vehicular Blockage on Backlayering Length in Tunnel Fire

Yu-Tsung Ho <sup>1,\*</sup> , Nobuyoshi Kawabata <sup>2</sup>, Miho Seike <sup>3</sup> , Masato Hasegawa <sup>4</sup>, Shen-Wen Chien <sup>5</sup> and Tzu-Sheng Shen <sup>5</sup>

- <sup>1</sup> Division of Mechanical Science and Engineering, Graduate School of Natural Science and Technology, Kanazawa University, Kakumamachi, Kanazawa 9201164, Japan
- <sup>2</sup> Faculty of Production Systems Engineering and Sciences, Komatsu University, Nu 1-3, Shicho-machi, Komatsu 923-8511, Japan; nobuyoshi.kawabata@komatsu-u.ac.jp
- <sup>3</sup> Graduate School of Advanced Science and Engineering, Hiroshima University, 1-5-1 Kagamiyama, Higashi-Hiroshima, Hiroshima 7398529, Japan; mihoseike@hiroshima-u.ac.jp
- <sup>4</sup> Department of Mechanical Engineering, National Institute of Technology, Ishikawa College, Kitacyujo, Tsubata 929-0392, Japan; mhase@ishikawa-nct.ac.jp
- <sup>5</sup> Department of Fire Science, Central Police University, No.56, Shujen Rd., Takang Vil., Kueishan District, Taoyuan City 33304, Taiwan; una179@gmail.com (S.-W.C.); una088@mail.cpu.edu.tw (T.-S.S.)
- \* Correspondence: hengbang@hibox.hinet.net; Tel.: +886-2-2888-1988



**Citation:** Ho, Y.-T.; Kawabata, N.; Seike, M.; Hasegawa, M.; Chien, S.-W.; Shen, T.-S. Scale Model Experiments and Simulations to Investigate the Effect of Vehicular Blockage on Backlayering Length in Tunnel Fire. *Buildings* **2022**, *12*, 1006. <https://doi.org/10.3390/buildings12071006>

Academic Editors: Víctor Yepes, Ignacio J. Navarro Martínez and Antonio J. Sánchez-Garrido

Received: 13 June 2022

Accepted: 11 July 2022

Published: 13 July 2022

**Publisher's Note:** MDPI stays neutral with regard to jurisdictional claims in published maps and institutional affiliations.



**Copyright:** © 2022 by the authors. Licensee MDPI, Basel, Switzerland. This article is an open access article distributed under the terms and conditions of the Creative Commons Attribution (CC BY) license (<https://creativecommons.org/licenses/by/4.0/>).

**Abstract:** This study used model experiments and numerical simulations to investigate the backlayering length of a vehicle-blocked tunnel fire. The experimental setup included two types of obstacles (low obstacles and high obstacles), as well as three configurations: no obstacles, one side with a car obstacle, and two sides with a car obstacle. If there were vehicles on one side of a lane, it would have little effect on the elongation of the backlayer length. When there were vehicles on both sides of a lane, the elongation of the backlayer length was greatly reduced. In addition, the effects of the vehicular blockage ratio and blockage configuration on the properties of the backlayering length were investigated. We created Pattern A, where fire is was in the center, and Pattern B, where fire was on the side of the tunnel. In Pattern A, almost all obstacles could be approximated using the formula. When the vehicle blockage ratio of a single lane was small, an approximation formula for Pattern B was applicable. However, if the distance between stationary vehicles on the upstream side of the fire source was small, the backlayering length could have been longer than in the case with no vehicular blockage.

**Keywords:** tunnel fire; backlayering length; thermal fume; vehicular blockage

## 1. Introduction

The movement of smoke or a hot gas against the direction of a tunnel's ventilation flow is called the backlayer. The backlayering length  $L_b$  of a thermal fume is defined as the horizontal distance between the front of the reverse smoke flow and the fire source. The measurement of ventilation control in the event of a fire is different in Europe and Japan. In Europe, longitudinal ventilation considers the velocity of 3 m/s to prevent backlayering [1], but this changes to the velocity of 1 m/s when water spray is activated or when there is a heavy traffic jam. In Japan, the ventilation velocity is 2 m/s [2], and when there is a heavy traffic jam, the jet fan is reversed to quickly set the ventilation velocity to 0 m/s [3–5], maintaining smoke in a stratified state along with the ceiling and maintaining an evacuation environment under the smoke layer.

Figure 1 shows the ventilation mode in a longitudinally ventilated tunnel in Europe and Japan with and without a traffic jam and the corresponding evacuation scenarios. As shown in Figure 1a, in the condition without a traffic jam, the ventilation velocity of 3 m/s

adopted in Europe would lead to the smoke layer hardly spreading upstream of the fire site, so safety can be ensured, but the downstream of the fire site would be filled with smoke at an early stage, and a safe evacuation environment cannot be expected. As shown in Figure 1b, in the condition without a traffic jam, the ventilation velocity of 2 m/s adopted in Japan would lead to the smoke layer spreading slower than the evacuee's walking speed, so safety can be ensured upstream of the fire site. Downstream of the fire site, although the smoke density near the road floor would be lower than that at 3 m/s, there is some possibility of evacuation, but it cannot be a safe evacuation environment. As shown in Figure 1c, in the condition of traffic jams, since the velocity of backlayering is close to the walking speed of the evacuees and the backlayering gradually drops, fast evacuation is required. In addition, although the condition of the downstream side is considerably improved, the smoke diffusion would also quickly spread to the road floor, so it cannot be considered that the downstream side is a safe space, and extremely quick evacuation is still required. As shown in Figure 1d, in the condition of traffic jams, it is assumed that the smoke is diffused both upstream and downstream, and the vehicles are almost stopped. Since the longitudinal ventilation velocity is 0 m/s, the smoke is stratified and spreads upstream and downstream along with the ceiling. Additionally, the velocity would be around 2 m/s when the gradient is 0%. Moreover, smoke would descend on the road floor at a point 200 m to 300 m away from the fire site about 10 min after the fire first occurred, and the descending smoke would flow and turn back to the fire source. Therefore, quick evacuation is required at an early stage. In view of the above, better understanding of the characteristics of backlayering, especially in conditions of traffic jams, is necessary.

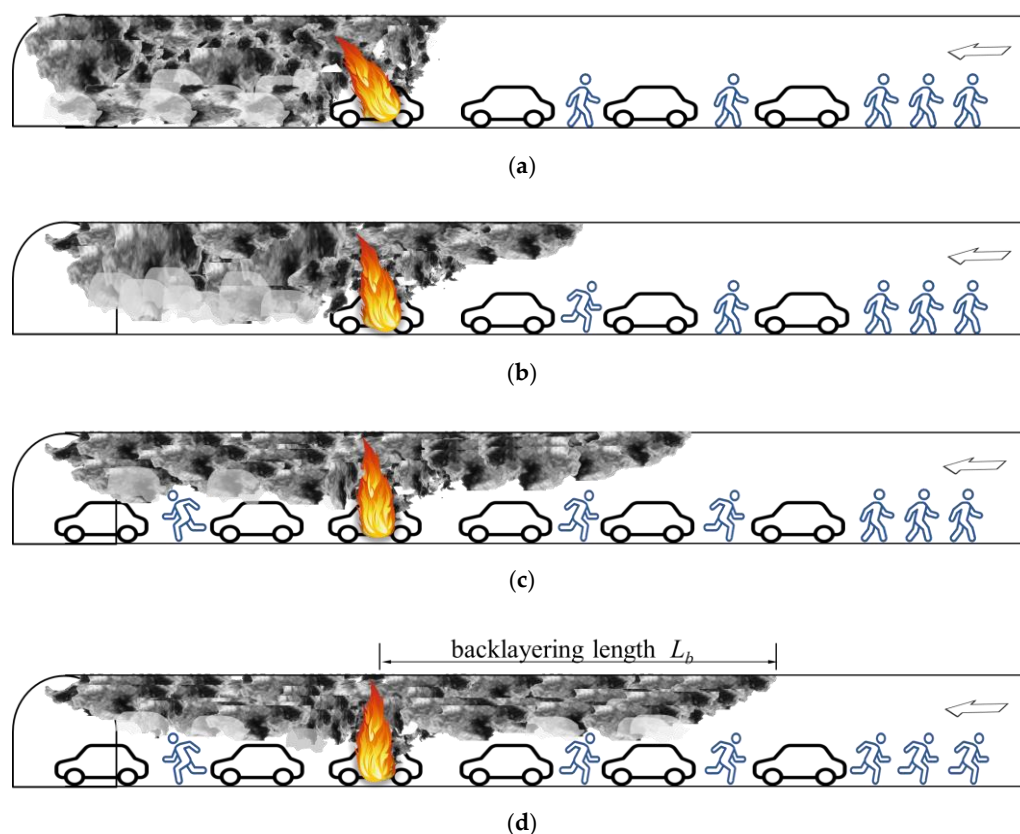


**Figure 1.** Longitudinal ventilation systems used in tunnels: (a) No traffic jam before the fire ( $U_m = 3$  m/s); (b) No traffic jam before the fire ( $U_m = 2$  m/s); (c) Traffic jam before the fire ( $U_m = 1$  m/s); (d) Traffic jam before the fire ( $U_m = 0$  m/s).

Although most research has focused on critical velocity, some studies have investigated the characteristics of backlayering length [6–13]. However, the effect of stranded vehicles

has not been taken into account in many of these studies. In the case of one-way traffic tunnels, many vehicles will be stranded on the side of the backlayering flow of dense smoke due to fire accidents, and these vehicles will affect the laminar flow of the dense smoke. Hence, it is crucial to clarify the effect of stranded vehicles on the backlayering length. There have been some studies on the impact of vehicular blockage on the backlayering length [14–21]. In these studies investigating the effect of obstacles on the backlayering length, there was one obstacle [17,18,20,21] or an obstacle such as a train [16,19]. Li et al. (2010) conducted a dimensional analysis of the theoretical formula and experimental formula regarding  $U_{cr}$  and  $L_b$  suggested in the past and conducted experiments with two types of tunnels (Tunnel A: square shape, 12 m (L)  $\times$  0.25 m (W)  $\times$  0.25 m (H); Tunnel B: horseshoe shape, 12 m (L)  $\times$  0.45 m (W)  $\times$  0.39 m (H)) [16]. A revised formula for a dimensionless heat release rate  $HRR$  was also proposed. They conducted the experiments with a simulated train obstacle in Tunnel B, which occupied 20% of the tunnel space, and proposed the relationship between  $U_{cr}$  and  $L_b$  using a Richardson number  $Ri$  and the dimensionless  $HRR$  in the case of a train obstacle. However, the  $L_b$  in the case of stagnant car congestion is different from that of a train because there are some air-filled spaces in the case of congestion in a road tunnel. Tang et al. (2013) conducted a dimensional analysis of the theoretical formula and experimental formula regarding  $U_{cr}$  and  $L_b$ . Their results were consistent with those of Li et al. (2010) [16]. Based on their experiments with the tunnel (rectangular shape, 72 m (L)  $\times$  1.5 m (W)  $\times$  1.3 m (H), made from glass), they proposed a revised formula by including the tunnel's cross-sectional area. One simulated bus obstacle was within reach of the fire source in the tunnel, and the relationship between the  $U_{cr}$  and the  $L_b$  in the case of a bus obstacle was revised by including the tunnel's cross-sectional area. Unlike this study, they used a bus as the obstacle and did not consider stagnant car congestion, as in Li et al. (2010) for the same reason. Zhang et al. (2016) conducted a dimensional analysis of the theoretical formula and experimental formula regarding  $U_{cr}$  and  $L_b$  [19]. Their results are in line with those of Li et al. (2010) [16]. One simulated train obstacle (6–18 m (L)  $\times$  1.5 m (W)  $\times$  1.3 m (H)) was set in the tunnel and was within reach of the fire source. The relationship between  $U_{cr}$  and  $L_b$  in the case of a train obstacle was revised by including the tunnel's cross-sectional area. In their study, they did not consider stagnant car congestion. Lee and Tsai (2012) investigated  $U_{cr}$  for stagnant car congestion through model-scale experiments (Tunnel A: 7 m (L)  $\times$  0.6 m (W)  $\times$  0.6 m (H); Tunnel B: 7 m (L)  $\times$  0.6 m (W)  $\times$  0.4 m (H)) with a coating 10 mm thick (the ceiling, floor, and side walls) and transparent glass 6 mm thick (another vertical side) [22]. CFD analysis was conducted to calculate the influence of the congestion. In the tunnel, there were two or three in the small, medium, and large stagnant car models. They proposed a revised equation for  $U_{cr}$  by including occupation by obstacles but did not take  $L_b$  into account. Fire experiments for  $L_b$  have not been conducted in the case of stagnant congestion by cars.

In view of the above, there are few studies on the effect of stagnant car congestion on  $L_b$ . Table 1 is a list of some studies on backlayering length. Because  $L_b$  will affect the safety of evacuation and rescue, and because in an actual tunnel fire, there may be stagnant car congestion, it is necessary to further investigate the effect of stagnant car congestion on  $L_b$ . In Section 2, the tunnel model established in this study, the measurement system for the temperature and the smoke, and the design of the fire source are described. Section 3 investigates the effect of vehicle blockage configuration and height on  $L_b$  through experiments and simulations. Section 4 further investigates the effect of the vehicle blockage ratio on the backlayering characteristics. In addition, an approximation formula is presented, along with a verification and discussion of the results. Finally, the findings and conclusions of this study are presented.

**Table 1.** List of studies on backlayering length.

Years	Research Topics	Authors	Research Methods	Obstacle Condition
1991	Investigation of Fire-Induced Smoke Movement in Tunnels and Stations: An Application to the Paris Metro [6].	Vantelon, J.P.; Guelzim, A.; Quach, D.; Son, D.K.	Experimental method	No obstacles
1994	Study Report on Fire Performance in Special Space of Use of Underground Space [7].	Saito, N.; Sekizawa, A.; Yamada, T.; Yanai, E.; Watanabe, Y.; Miyazaki, S.	Experimental method	No obstacles
2005	Definition and Experimental Evaluation of the Smoke “Confinement Velocity” in Tunnel Fires [8].	Vauquelin, O.; Telle, D.	Experimental and simulation methods	No obstacles
2008	Critical Wind Velocity for Arresting Upwind Gas and Smoke Dispersion Induced by Near-Wall Fire in a Road Tunnel [9].	Hu, L. H.; Peng, W.; Huo, R.	Experimental and simulation methods	No obstacles
2012	Backlayering Distance of Thermal Fume in Tunnel Fire Experiments Using a Large-Scale Model [10].	Minehiro, T.; Fujita K.; Kawabata, N.; Hasegawa, M.; Tanaka, F.	Experimental and simulation methods	No obstacles
2016	Thermal Smoke Back-layering Flow Length with Ceiling Extraction at Upstream Side of Fire Source in a Longitudinal Ventilated Tunnel [11].	Tang, F.; Li, L.J.; Mei, F.Z.; Dong, M.S.	Experimental and simulation methods	No obstacles
2018	Critical Velocity and Backlayering Distance in Tunnel Fires with Longitudinal Ventilation Taking Thermal Properties of Wall Materials into Consideration [12].	Tanaka F.; Takezawa K.; Hashimoto Y.; Moinuddin K.A.M.	Experimental method	No obstacles
2021	Experimental Study of Back-layering Length and Critical Velocity in Longitudinally Ventilated Tunnel Fire with Various Rectangular Cross-sections [13].	Zhang T.; Wang G.; Li J.; Huang Y.; Zhu K.; Wu K	Experimental method	No obstacles
1998	Study of Ventilating Operation During Fire Accident in Road Tunnels With Large Cross Section [14].	Kawabata, N.; Wang, Q.; Yagi, H.; Kawakita, M.	Simulation method	More than two obstacles
2006	Influence of Vehicular blockage on Backlayering Characteristics of Fire Plume in a Large Cross Section Tunnel [15].	Kunikane, Y.; Kawabata, N.; Yamada, T.; Shimoda, A.	Simulation method	More than two obstacles
2010	Study of Critical Velocity and Backlayering Length in Longitudinally Ventilated Tunnel Fires [16].	Li, Y.Z.; Lei, B.; Ingason, H.	Experimental method	An obstacle
2013	Effect of Blockage-Fire Distance on Buoyancy Driven Backlayering Length and Critical Velocity in a Tunnel: An Experimental Investigation and Global Correlations [17].	Tang, W.; Hu, L.H.; Chen, L.F.	Experimental method	An obstacle
2015	Numerical Study of the Effect of Blockage on Critical Velocity and Backlayering Length in Longitudinally Ventilated Tunnel Fires [18].	Gannouni, S.; Maad, R.B.	Simulation method	An obstacle
2016	An Experimental Investigation on Blockage Effect of Metro Train on the Smoke Back-layering in Subway Tunnel Fires [19].	Zhang, S.; Cheng, X.; Yao, Y.; Zhu, K.; Li, K.; Lu, S.; Zhang, R.; Zhang, H.	Experimental method	An obstacle
2018	Effect of blockage ratio on backlayering length of thermal smoke flow in a longitudinally ventilated tunnel [20].	Meng, N.; Liu, X.; Li, X.; Liu, B.	Experimental method	An obstacle
2018	Experimental Study on Backlayering Length of Thermal Smoke Flow in a Longitudinally Ventilated Tunnel with Blockage at Upstream of Fire Source [21].	Meng, N.; Yang, W.; Xin, L.; Li, X.; Liu, B.; Jin, X.	Experimental method	An obstacle

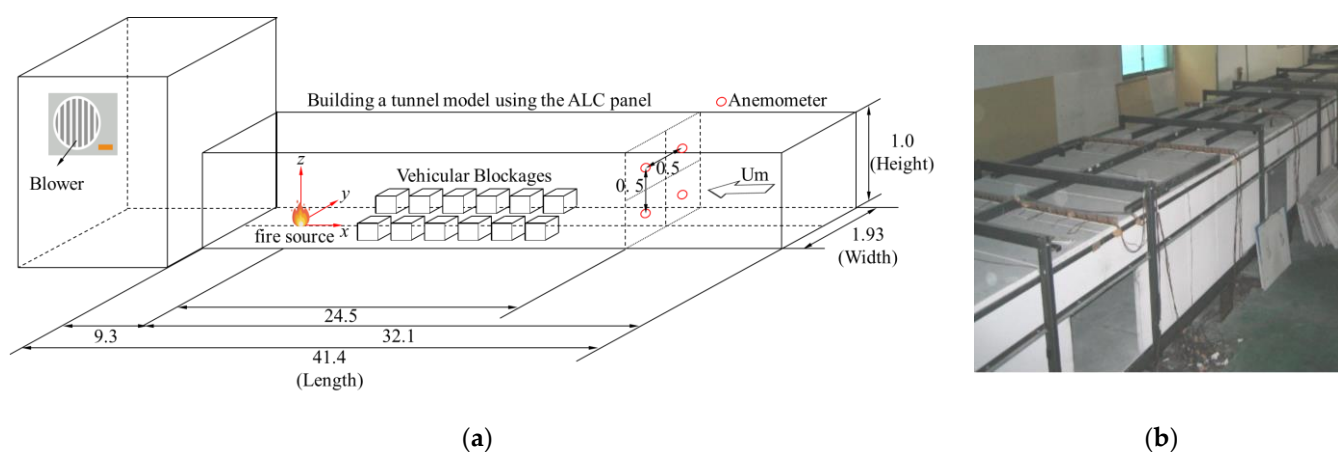
## 2. Model Tunnel and Experimental Procedure

### 2.1. Scale Model Tunnel

The model tunnel used in this study experiment was designed to be 1/5 of the actual tunnel. Table 2 is a list that converts the scale of model tunnels to actual tunnels. The model’s cross-section was a rectangular shape, and the model was designed based on laws of similarity. The model tunnel was constructed from an autoclaved lightweight concrete panel (ALC panel) with a thickness of 0.035 m. The experimental longitudinal velocity  $U_m$  ranged from 0.15 m/s to 1.22 m/s, the Froude number ranged from 0.05 to 0.39, and the Reynolds number ranged from  $5.68 \times 10^4$  to  $1.03 \times 10^5$ . Figure 2 shows the model of a tunnel ( $x$ -axis, 41.4 m (L);  $y$ -axis, 1.93 m (W);  $z$ -axis, 1 m (H)).

**Table 2.** List of model tunnels and actual tunnels.

Type	Experimental Model	Actual Tunnel
Section shape	rectangular	rectangular
The width of the tunnel $W$ (m)	1.93	10
The height of the tunnel $H$ (m)	1	5
Tunnel cross-section area $A_t$ (m <sup>2</sup> )	1.93	50
Froude number $Fr$	0.07–0.39	0.07–0.39
Dimensionless average heat re-release rate $Q^*$	0.072	0.072
Material (near the fire source)	ALC	concrete
Biot number $Bi$	42.7–52.8	44.7–61.8
Fourier numbers $Fo$	$6.41 \times 10^{-8}$	$1.72 \times 10^{-8}$

**Figure 2.** Model tunnel structure and compositional diagram: (a) Dimensions and configuration of the tunnel model (unit: meters); (b) Photo of tunnel model.

Figures 3 and 4 are schematics of the vehicular configuration in the  $x$ - $y$  section view and in the  $y$ - $z$  sectional view, respectively, with two lanes in the tunnel models. The blue arrow represents the direction of longitudinal velocity. The vehicular blockage in the experiment was a container made of calcium silicate. The scales of both tunnels and vehicle obstacles in the model in this study were 1/5. In the model tunnel, we simulated large buses with cuboid obstacles, 0.5 m in height, 0.567 m in width, and 1.26 m in length (the actual size is 2.5 m in height, 2.835 m in width, and 6.3 m in length). In addition, there were also relatively tall cuboid obstacles to simulate trucks. The model trucks were 0.7 m in height, 0.567 m in width, and 1.26 m in length (the actual size is 3.5 m in height, 2.835 m in width, and 6.3 m in length). Upstream from the fire source, obstacles were placed, including passenger cars as low obstacles and buses as high obstacles. The experimental setup included two types of obstacles, low obstacles and high obstacles, as well as three configurations with no obstacles  $M0$ , one side with a car obstacle  $M1$ , and two sides with a car obstacle  $M2$ . In experiments  $M1$  and  $M2$ , the distance between the front of the two vehicles was 2 m and 4 m, respectively. The first vehicle was placed at a distance of 1 m from the fire source and 0.2 m from the nearest tunnel side wall. In reality, more vehicles would be inside the tunnel to create obstacles. The total length of vehicular blockage set in this study was 24.3 m for experiment  $M1$  and 22.3 m for experiment  $M2$ . A comparison of  $M0$ ,  $M1$  and  $M2$  experiments and simulations is discussed in Section 3.3.

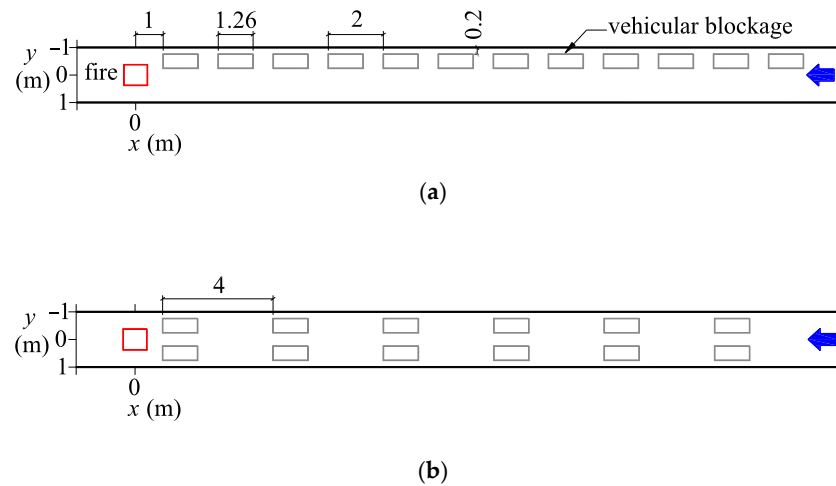


**Figure 3.** Schematic of the configurations with vehicular blockages: (a) One side with vehicular blockage, M1; (b) Both sides with vehicular blockage, M2.

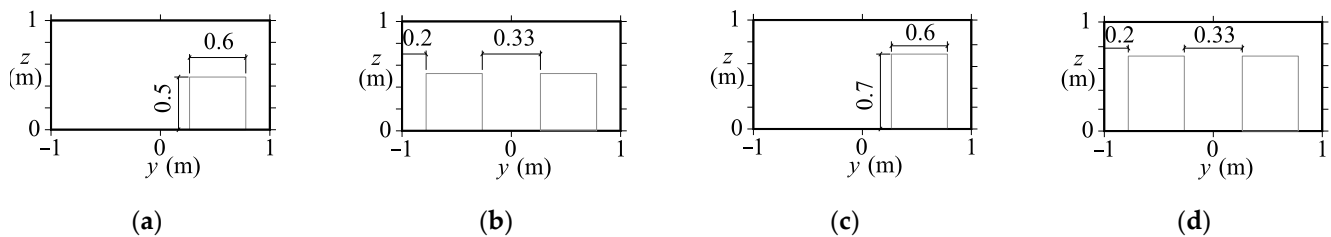


**Figure 4.** Schematic of vehicular configurations and heights in the model: (a) Low obstacles in M1; (b) Low obstacles in M2; (c) High obstacles in M1; (d) High obstacles in M2.

In the numerical simulations of M1 and M2, the distances between the fronts of the two vehicles were, respectively, 2 m and 4 m. The first vehicle was 1 m away from the fire source and 0.234 m away from the nearest tunnel side wall. In reality, vehicles traveling in a tunnel may include buses, trucks, and small cars of different dimensions; this study used lower and higher vehicle models for the simulation, including different vehicular patterns, vehicular heights, and longitudinal ventilation velocities. The convective heat ratio of a gasoline pool fire accounts for 40–60% of the caloric value [23]. In this study, the convective  $HRR$  was set as 60% of the heat of complete combustion, and  $L_b$  was measured in the quasi-steady state. In the experiment, the average distance in the  $y$ -direction was calculated as  $L_b$ .

## 2.2. Temperature and Smoke Measurement System

The model experiment in this study used K-type thermocouples to measure the temperature of the thermal fume in the tunnel. The thermocouples near the fire source also detected radiated heat in addition to the convective heat, thus rendering them unable to measure the correct  $L_b$ . Therefore, in places close to the fire source, a laser irradiation system parallel to the ceiling was installed to deduce the  $L_b$ . At locations further from the fire source, thermocouples were installed to measure the convection heat. This study affixed thermocouples at the ceiling (at intervals of 1 m) to measure  $L_b$ . The thermocouples (0.1 mm in diameter) were used to measure the internal temperature distribution. The data collector received the transmitted temperature measurements at 1 s intervals. At locations near the ceiling, thermocouples were installed 20 mm away to measure the temperature. As the experimental values of  $L_b$  were mostly calculated based on the measurements along the centerline (laser beam and thermocouple) [6,10,12,16,19], this study set the thermocouples at 1 m intervals along the centerline and nine thermocouples at 2 m. As

shown in Figure 5, the fire source was placed on the floor position at the origin, and a total of 169 thermocouples were installed on the ceiling, including 8 along the  $z$ -axis and 122 along the  $x$ -axis. In all, there were 291 temperature measurement points. The measurement of  $L_b$  used thermocouples with  $z = 0.90$  m and  $z = 0.98$  m at intervals of 1 m in the  $x$ -direction.

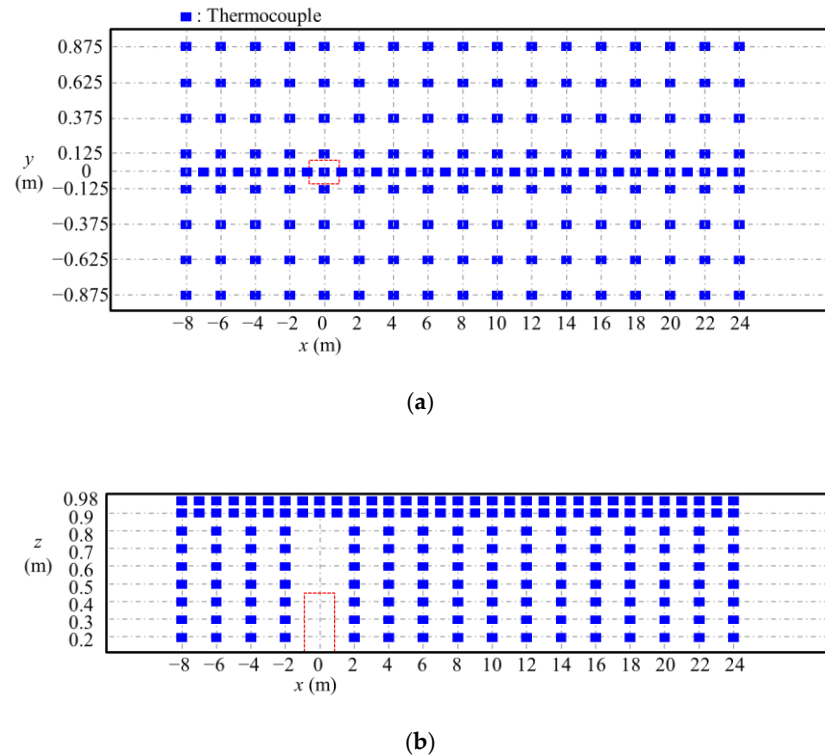


**Figure 5.** Configuration diagram of the thermocouples: (a) Thermocouples on the ceiling ( $z = 0.98$  m); (b) Thermocouples on the wall in the vertical direction ( $y = 0$ ).

To measure the fumes' flow dispersion and movement near the fire source, a laser system for measuring the smoke concentration was installed in the experimental tunnel. The measurement of smoke densities entailed installing light emission and reception devices in holes in the walls. Light emission and reception devices were installed every 0.2–0.1 m from the ceiling down to the ground, at six locations. Along the length of the tunnel, light emission and reception devices were installed at  $x = -5.4$  m, 6.6 m, and 12.6 m; 18 devices for smoke measurement were used. To confirm the accuracy of the equipment, the equipment was calibrated with a glass. The measurement interval time was set to 1 s. The smoke concentration signal converted the emitted light it received to voltages, so we could determine the smoke concentration according to the voltage variations. The same initial voltage at the beginning of the experiment was used for all receivers. During the experiment, smoke from the fire source would block some of the light shone from the emitters to the receivers, causing the receiver's voltage to decrease, indicating an increased concentration. The distance between the position where the thermal fume temperature was  $5^\circ\text{C}$  higher than the ambient temperature (see Figure 6) and the fire source was regarded as the  $L_b$ .

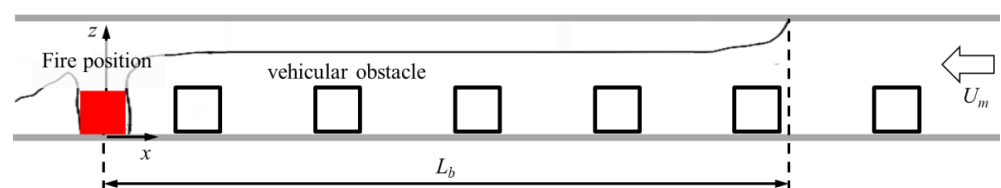


**Figure 6.** Schematic diagram of the definition of  $L_b$  of the vehicular blockage in the  $x$ - $z$  section view.

### 2.3. Heat Release Rates

To measure the  $L_b$  and  $U_m$  in the quasi-steady state range, this study used pool fires for the simulation and observed the heat release rates through the rate of fuel reduction. In the simulation, the fire source was at a distance of 9.3 m from the cabin's opening and 32.1 m from the upper section of the tunnel (see Figure 2). A 0.15 m<sup>2</sup> stainless steel oil pan was placed at the middle section of the tunnel (0.97 m from the tunnel wall), and it was filled with *n*-heptane (1500 g) and water (3000 g). An electronic scale was used to measure the fuel reduction rate  $R_f$  (g/s), which was then multiplied by the fuel's unit heat value (for *n*-heptane, heat value = 44.56 kJ/g). The theoretical heat release rate  $Q$  (kW) was then calculated. The result was close to that of previous studies [16,24]. An additional radiometer was placed inside the tunnel 1.5 m from the upper section of the fire source and 0.2 m above the ground to measure the heat value every 0.2 s. The smoke generated from the fuel used in this study, *n*-heptane, had a low concentration. The measuring point was located windward the of the fire source, without affecting the radiometric measurements. Figure 7 shows the initial longitudinal velocity  $U_{mi} = 0.71$  m/s,  $Q_m = 153$  kW, and the time change in the longitudinal velocity of ventilation  $U_m$ .

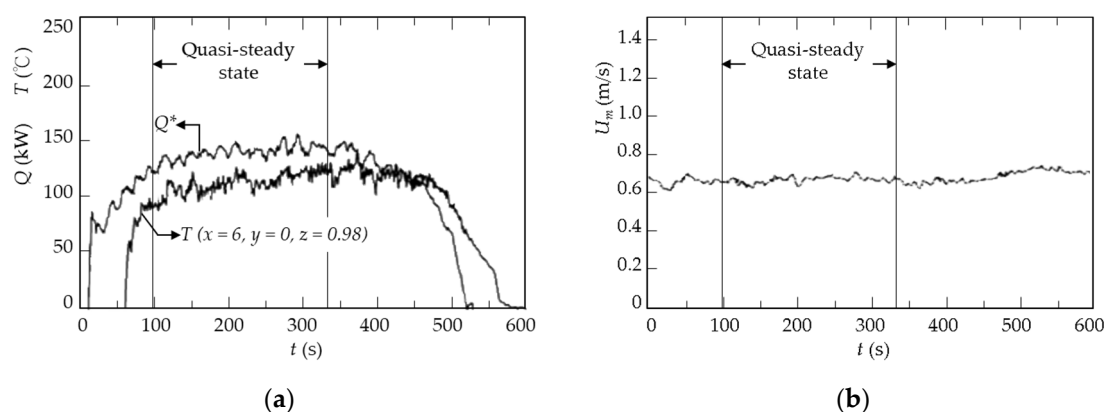


**Figure 7.** Initial longitudinal velocity  $U_{mi} = 0.71$  m/s,  $Q_m = 153$  kW ( $Q_m^* = 0.072$ ): (a) HRR and temperature distributions; (b) Longitudinal velocity.

The experiments in this study were carried out using a Climomaster anemometer manufactured by KANOMAX Corporation. The average initial longitudinal velocity,  $U_{mi}$ , was measured using anemometers 30 s before ignition. Four anemometers were installed to measure the  $U_m$ , taking measurements at 1 s intervals. Two anemometers were set near the fire source ( $x = 24.5$  m;  $z = 0.25$  m;  $x = 24.5$  m,  $z = 0.75$  m), one at  $y = 0.5$  m, and another at  $-0.5$  m each. The average  $U_m$  maintained a stable value before ignition, but the hot air after ignition lowered its value.  $U_m$  was then measured every 30 s, and the average value was calculated.

## 3. Investigating the Effects of the Configuration and Height of Vehicular Blockages

### 3.1. Simulator and Verification of the Grid Size

The simulations in this study used the original code (Fireles) developed by one of the authors [14]. In around 2002, Fireles conducted large-scale fire experiments on the Shin-Tomei Expressway connecting Tokyo and Nagoya as a CFD tool for tunnel disaster prevention. According to the experiments, it was verified that Fireles has good quantitative prediction accuracy in terms of temperature distribution [25], smoke concentration distribution [25], backlayering characteristics [25], heat release rate estimation [25], and smoke descent characteristics [26]. Since then, it has been used as a standard CFD tool for fire prevention studies in major tunnels in Japan.

The thermal plume in a tunnel fire is typically very hot and is associated with a cubic expansion of air volume. Therefore, the airflow needs to be treated as compressible. The three-dimensional large eddy simulation (LES) turbulence model is applied to the velocity

field under the condition that the temperature variation is much less than the variation in velocity. The following governing equations are employed.

Continuity Equation (1):

$$\frac{\partial \rho}{\partial t} + \nabla(\rho v) = 0 \quad (1)$$

Navier-Stokes Equation (2):

$$\frac{\rho Dv}{Dt} = -\nabla P + \nabla \sigma + \rho g \quad (2)$$

where

$$\frac{D}{Dt} = \frac{\partial}{\partial t} + (v \nabla), \sigma = \rho \nu_t \{ (\nabla v) + (\nabla v)^T \} \quad (3)$$

Energy Equation (4):

$$\rho \frac{DC_v T}{Dt} = \nabla \left( \frac{C_v \rho \nu_t}{\sigma_h} \nabla T \right) + Q_h - P(\nabla v) \quad (4)$$

Status Equation (5) of perfect gas:

$$\rho = \frac{P}{RT} \quad (5)$$

Diffusion Equation (6) of smoke:

$$\rho \frac{DC}{Dt} = \nabla \left( \frac{\rho \nu_t}{\sigma_c} \nabla C \right) + Q_c \quad (6)$$

where  $\sigma_h$  is the turbulent Prandtl Number (0.5 in the present study), and  $\sigma_c$  is the turbulent Schmidt Number (0.5 in the present study). The coefficient of turbulent viscosity  $\nu_t$  is determined by

$$\nu_t = (C_s \Delta)^2 \left\{ \frac{1}{2} \left( \frac{\partial v_i}{\partial x_j} + \frac{\partial v_j}{\partial x_i} \right)^2 - \frac{2}{3} (\nabla v)^2 \right\}^{(1/2)} \quad (7)$$

where  $C_s$  is the Smagorinsky Constant, and  $\Delta$  is the size of the filter and is given by  $(\Delta x \times \Delta y \times \Delta z)^{1/3}$ .

Pressure  $P$  is defined as

$$P = P_0 + p_0 + p \quad (8)$$

where  $p_0$  and  $p$  are much lower than the atmospheric absolute pressure  $P_0$ , which is in the order of 105 Pa. Therefore, Equation (5) can be rewritten as

$$\rho \approx \frac{P_0}{RT} \quad (9)$$

and

$$\frac{1}{\rho} \frac{D\rho}{Dt} = -\frac{1}{T} \frac{DT}{Dt} \quad (10)$$

Substituting Equation (10) into the continuity Equation (1) and energy Equation (4), the continuity equation becomes

$$\nabla v = \frac{1}{C_p \rho T} \left\{ \nabla \left( \frac{C_v \rho \nu_t}{\sigma_h} \nabla T \right) + Q_h \right\} \quad (11)$$

and the Navier–Stokes Equation (2) becomes

$$\frac{Dv}{Dt} = -\frac{1}{\rho} \nabla p + \frac{1}{\rho} \nabla \sigma + \frac{\rho - \rho_0}{\rho} g \quad (12)$$

where the third term on the right side of Equation (12) is a buoyancy term. Putting this term into Equation (9), we obtain the following equation by ignoring the terms involving  $p_0/P$  and  $p/P$ :

$$\frac{\rho - \rho_0}{\rho} g = \left(1 - \frac{T}{T_0}\right) g \quad (13)$$

According to the above discussion, the governing equation consists of the continuity Equation (11), the Navier–Stokes Equation (12), the energy Equation (4), the status Equation (9), the smoke diffusion Equation (6), and the turbulence model (7). The explicit Crank–Nicolson method is used for progressing time, and the simplified marker and cell (SMAC) method is adopted for determining pressure and velocity fields. Since the center difference scheme is usually used in LES, Fireles also applies the fourth-order accuracy central difference to describe the convection term of the Navier–Stokes equation. The third-order accuracy upwind difference scheme is applied to the convection term of the energy equation. A central difference scheme with second-order accuracy is employed to describe the spatial diffusion terms. The adjustable time-step method is used for computation under the Courant condition.

The dominant factors in the smoke backlayering phenomenon are the diffusion of smoke due to the longitudinal flow, the backflow area, the turbulent shear flow, and the endothermic heat from the hot airflow on the ceiling surface. Therefore, this section describes the boundary conditions on the wall surface used in Fireles.

First, for the velocity field, we considered the cell center in contact with the wall and divided it into three cases:

- (i) The laminar boundary layer.
- (ii) The wall function for a smooth wall involving in the turbulent boundary layer.
- (iii) The same as the surface roughness.

In the case of (i),  $u_i$  is assumed as the velocity in the direction along the wall at the center of the cell, the frictional stress  $\tau_w$  is obtained using the following formula:

$$\tau_w = \mu u_i / \delta \quad (14)$$

Here,  $\delta$  is the distance between the cell center and the wall.

In the case of (ii), the frictional stress is calculated by the following formula, following the wall law of a smooth wall.

$$\frac{u_i}{u_\tau} = \frac{1}{0.4} \ln \frac{\delta u_\tau}{\nu} + 4.1, \quad u_\tau = \sqrt{\frac{\tau_w}{\rho}} \quad (15)$$

Here,  $\nu$  is the kinematic viscosity of air.

In the case of (iii), it is assumed that the wall roughness  $\varepsilon$  is about the same as  $\delta$ , the logarithmic law of the wall in fluid dynamics is applied, and the frictional stress is obtained using the following equation:

$$\frac{u_i}{u_\tau} = 5.75 \log \frac{\delta}{\varepsilon} + 8.5 \quad (16)$$

The heat absorption condition to the wall gives the heat transfer coefficient  $h$ , but many empirical equations of the heat transfer coefficient have been proposed so far to show the relationship between the Bulk flow and the heat transfer coefficient in a circular tube or a flat plate and the cells in contact with each other. It takes some ingenuity to find the relationship between the wall and the wall.

In the Fireles, three heat transfer conditions can be selected:

- (i)  $h$  is a constant.
- (ii) The Yurges formula:

$$h = 5.92 + 3.95|U_i|/T_i \quad (17)$$

- (iii) Colburn's analogy.

where  $U_i$  and  $T_i$  are the velocity component and temperature along the wall in the center of the cell in contact with the wall, respectively. The Yurges formula is originally a relational formula between the velocity, the temperature, and the heat transfer coefficient outside the temperature boundary layer. The cell size was about 0.2 m, which was the same as the thickness degree of the temperature boundary layer, but in the case of a full-scale tunnel, it was judged to be applicable. However, since the cell size may be about 1 cm in a reduced model tunnel, the Yurges formula could not be applied as it is.

Like the Yurges formula, Colburn's analogy also uses frictional stress to determine the heat transfer coefficient from the ratio of the heat flow rate to the momentum flow rate in the Bulk flow outside the temperature boundary layer, but this flows in the cell in contact with the wall. The heat transfer coefficient is calculated using the ratio of the heat flow rate and the momentum flow rate, and the correction coefficient is further used. This method is intended for the case of a reduced model. Moreover, in this paper, the Yurges formula was applied to the simulation of the model scale tunnel, despite this being a large model tunnel with a reduction ratio of 1/5, and the cell size was several centimeters. This is because it was judged that the difference from the value outside the temperature boundary layer was not large.

The parameters used in the aforementioned governing equations for performing simulations are shown in Kawabata (2003) [26]. In this paper, we reexamined the reproducibility of the turbulent flow phenomenon. Table 3 shows the results of the examination of  $C_{sgs}$ . Since most of the measurements of the turbulent flow intensity of the flow in the rectangular duct were for the square duct, we also simulated the flow with the average velocity of 2 m/s in the square duct of 5 m square. These are the results shown for 60 s in a well-developed turbulent state. Each  $C_{sgs}$  and corresponding pipe friction coefficient  $\lambda$ , average velocity  $\bar{u}_c$  at the center of the cross section, and the turbulence intensity, while turbulent flow strength is larger than the grid size, is also shown in Table 3 with the condition of the wall roughness of 2 mm and the Reynolds number of 580,000.

**Table 3.** The results of this study on  $C_{sgs}$ .

$C_{sgs}$	$U_m$ (m/s)	Friction Factor $\lambda$	Average Velocity $\bar{u}_c$ (m/s)	Turbulence Intensity $\sqrt{u'^2}$ (m/s)
0.10	2.0	Unstable		
0.12	2.0	0.0169	2.48	0.0845
0.14	2.0	0.0178	2.45	0.0874
0.15	2.0	0.0179	2.47	0.1033
0.17	2.0	0.0129	2.93	0.0208
0.20	2.0	0.0129	2.93	0.0001

The calculation would diverge when  $C_{sgs}$  was 0.10. When  $C_{sgs}$  was in the range of 0.12 to 0.15,  $\bar{u}_c$  was 2.45 to 2.48 m/s and the turbulence intensity was 0.085 to 0.103, but when  $C_{sgs}$  was 0.17, the center velocity was 2.93 and the turbulence intensity was 0.0208. When  $C_{sgs}$  became 0.20, the turbulent intensity became almost 0, the fluctuation due to the vortex captured by the grid size was almost eliminated, and the velocity distribution became a shape close to the parabolic distribution without fluctuation like at the time of laminar flow, and it could not be considered as LES anymore.

From this analysis, it can be considered that  $C_{sgs}$  should be in the range of 0.12 to 0.15 in the case of the fourth-order precision center difference used in this study. On the other hand, in Fire Dynamics Simulator (FDS),  $C_{sgs}$  have a default value of 0.20. It could be that FDS adopts an alternative repeating between the second-order accurate leeward difference scheme and the second-order accurate upwind difference scheme. The coefficient of friction of full-scale tunnels has been reported as 0.016 to 0.036 [27]. In the present study, the coefficient of friction was in the range of 0.12 to 0.15 when  $C_{sgs}$  was 0.017 to 0.018. The value was close to the lower range in the result of Hong-Ming et al. (2002) [27]. This is because

except for the wall surface with a roughness of 2 mm, there were no other installations on the wall surface in our study.

Since the model tunnel dealt with in this study was about 1/5 of the size of the full-scale tunnel, we thought that the specifications for the full-scale tunnel could be applied, but since the grid division width ( $\Delta x, \Delta y, \Delta z$ ) was significantly different, we re-examined the dependency of the division width. Figure 8 also shows the change in the heat generation rate calculated from the fuel reduction rate assuming complete combustion, but there was not much change from 180 to 300 s, and the average was 194 kW. The vertical wind speed averaged 0.774 m/s between 180 and 300 s, with a change in the range of 0.75 m/s to 0.78 m/s. The grid division width ( $\Delta x, \Delta y, \Delta z$ ) was 44.25 m and 885 divisions, 1.93 m and 49 divisions, and 1.00 m and 31 divisions for Grid 0; 44.195 m and 699 divisions, 1.93 m and 43 divisions, and 1.00 m and 27 divisions for Grid 1; 44.284 m and 601 divisions, 1.93 m and 39 divisions, and 1.00 m and 23 divisions for Grid 2; and 44.3 m and 443 divisions, 1.93 m and 33 divisions, and 1.00 m and 19 divisions for Grid 3. Figure 8 shows the time course of each backlayering length. The finely divided Grids 0 and Grid 1 were almost the same and agreed well with the experimental results. Grid 2 and Grid 3 have shorter backlayering lengths, but the difference from Grid 0 was 2 m or less. When considering the influence of stagnant vehicles, it is easier to adjust the position setting of stagnant vehicles when the grid division width is small, so Grid 0 was used for the subsequent simulations. Table 4 lists the conditions used for the numerical simulations in this study.

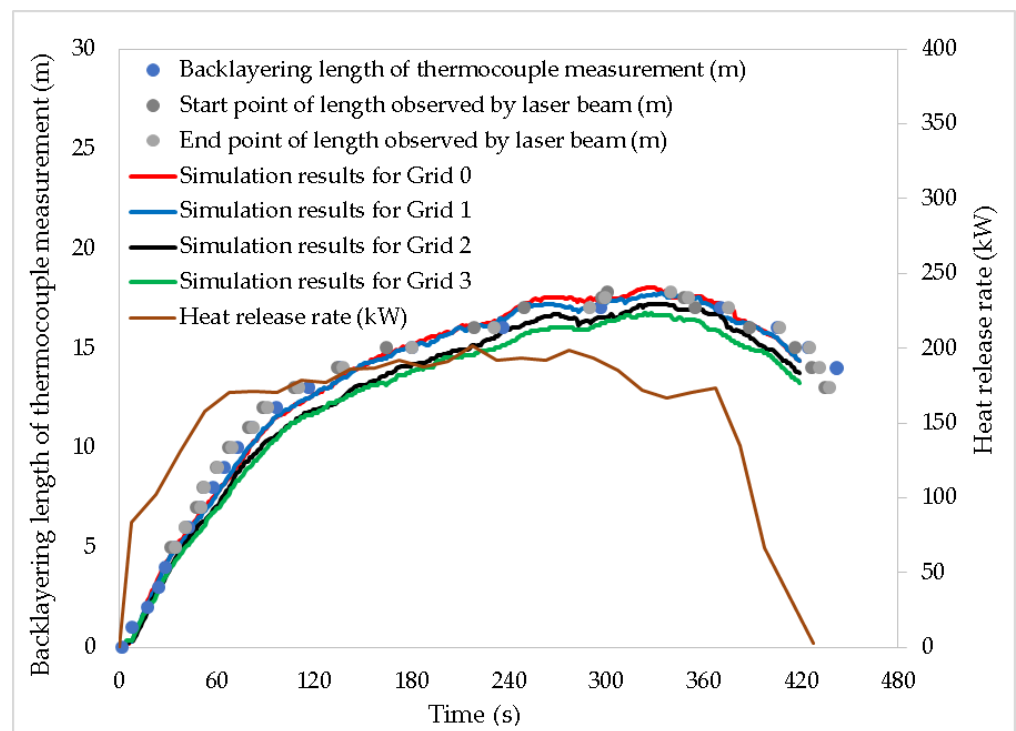


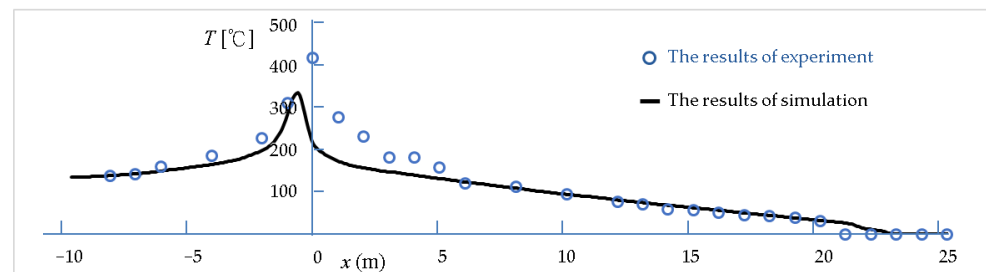
Figure 8. Grid independence test for the simulation.

Table 4. Conditions used for the numerical simulation.

Tunnel				Vehicular Blockage									
x		y		z		x		y		z			
Length		Width		Height		Length		Width		Low Height		High Height	
Grid number	Dim. (m)	Grid number	Dim. (m)	Grid number	Dim. (m)	Grid number	Dim. (m)	Grid number	Dim. (m)	Grid number	Dim. (m)	Grid number	Dim. (m)
885	44.25	49	1.93	31	1	25	1.25	13	0.51	15	0.48	22	0.71

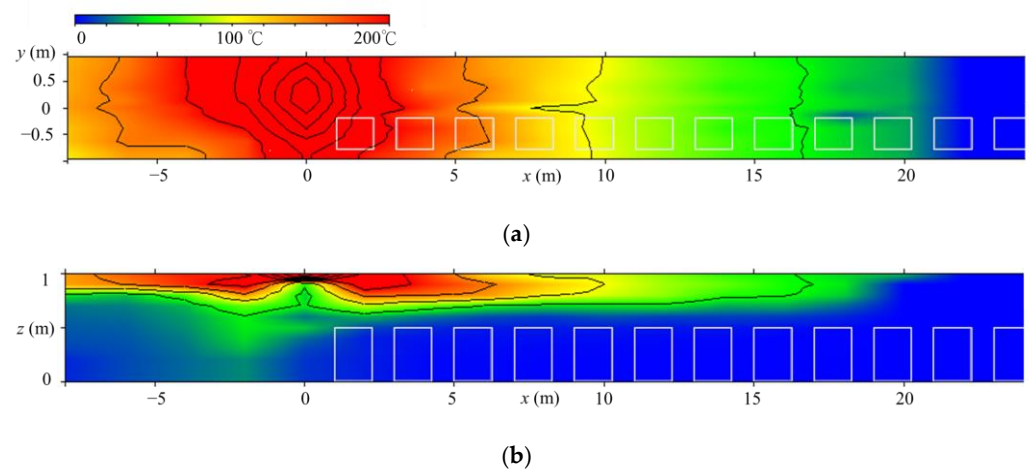
### 3.2. Comparison of the Experimental Results and Simulation Results

Figure 9 shows a comparison between the temperature distribution experiment's results in the  $x$ -direction and the simulation results of the model at  $z = 0.98$  m, taking MIL as a vehicle with a height of 0.5 m. In the experiment, the heating velocity was  $Q_m = 161$  kW, the longitudinal velocity was  $U_m = 0.421$  m/s, and the time was a mean value between 200 and 260 s in the quasi-steady state. The simulation was conducted under the same conditions as the experiment. In Figure 9, the circle indicates the experimental value, and the curve indicates the simulation results. In areas more than 3 m from the side of the backlayering thermal fume (right side) of the fire source, the distribution of the experimental results and the simulation was quite close. If the backlayering length was about 1 m longer than that in the simulation and the measurement points were set at every 1 m in the experiment, the results would be quite close. In areas near the fire source (0–2 m), the temperature in the experiment was high, because radiant heat was not considered in the simulation.



**Figure 9.** The temperature distribution experiment's result in the  $x$ -direction compared with the results of the simulation model;  $z = 0.98$  m,  $Q_m = 161$  kW,  $U_m = 0.421$  m/s,  $t = 200$  to 260 s.

Figures 10 and 11 compare the average value of the temperature distribution from 200 to 260 s. Figure 10 shows the experimental results, and Figure 11 shows the simulation results, representing (a) the horizontal plane at  $z = 0.98$  m and (b) the longitudinal section at  $y = 0$ , respectively. In the longitudinal section shown in Figure 10b, there was no fire plume rising from the fire panel, because the measurement points with  $x = 0$  were not set due to their direct contact with the flame, except at  $z = 0.98$  m. According to these figures, the experiment and the simulation agreed with each other, except for the area where the effect of the radiant heat near the fire point was great. Furthermore, in Figure 10a, a position with a value lower than the value at  $y = 0$  is shown, but this measurement value was excluded from the experimental results shown in Figure 9. After a comparison with other cases (*M1H*, *M2L* and *M2H*), it was verified that the simulation results were roughly consistent with the experimental results.



**Figure 10.** Experimental results of the temperature distribution in the central longitudinal section;  $Q_m = 161$  kW,  $U_m = 0.421$  m/s,  $t = 200$  to  $260$  s: (a)  $z = 0.98$  m; (b)  $y = 0$ .

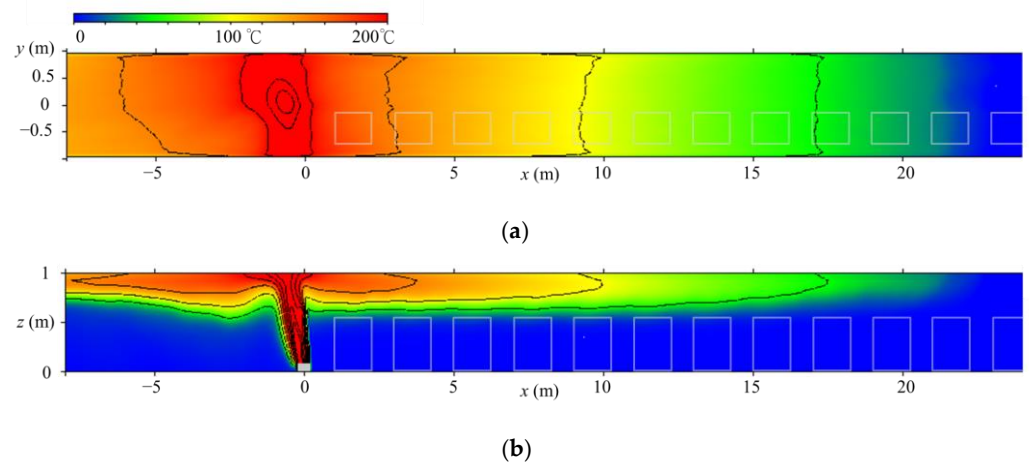


**Figure 11.** Simulated results of the temperature distribution in the central longitudinal section;  $Q_m = 161$  kW,  $U_m = 0.421$  m/s,  $t = 200$  to  $260$  s: (a)  $z = 0.98$  m; (b)  $y = 0$ .

In the comparison between the model experiment and the simulation, the reason for the difference in the temperature distribution near the fire source was that the simulation was not affected by radiant heat, as mentioned above, but this is further explained below. Figure 12 shows that the fire plume tilted due to the upstream longitudinal velocity, and Figure 9 shows that the tilt angle of the fire panel surface was about  $40^\circ$  when the fire plume reached the maximum temperature of the ceiling at  $x = -0.6$  m. Therefore, the radiant heat on the upstream side of the fire source would have a great effect on the ceiling, and the radiant heat on the downstream side would have a great effect on the floor. The temperature of the thermocouple near the ceiling on the upstream side was higher than that of the surrounding thermals, while the temperature of the thermocouple on the downstream side was still high due to the radiant heat of the fire plume, despite the low air temperature under the thermals on the downstream side.

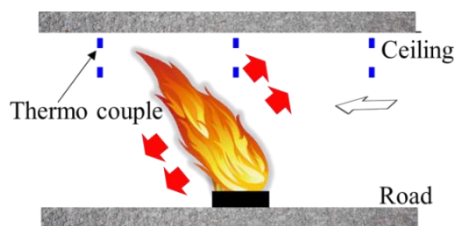


Figure 12. Tilt of the fire plume due to the upstream longitudinal velocity.

3.3. Comparing the Effects of the Configuration and Height of Vehicle Blockage

Figure 13 shows the simulation and experimental results of the correlation between the backlayering length  $L_b$  and  $Q^{*1/3}/Fr$ . The experimental and simulation results of the scale model tunnel were in conformity. The results showed that vehicle height had less effect on the backlayering length when the stationary vehicles were arranged in a line. Moreover, when we compared M0 with M1L and M1H, the slope of their curves were roughly the same when  $L_b^*$  was less than 5, but when  $L_b^*$  was greater than 5, the slope of the curves of M1L and M1H were smaller. In addition, when the vertical axis  $Q^{*1/3}/Fr$  was the same, the backlayering length of M0 was longer. Furthermore, the approximation curve was calculated from the results for  $L_b^* > 5$ . When the stationary vehicles were in two columns M2L and M2H, the backlayering length propagation characteristic was reduced by the blocking effect induced by the vehicle model, and that of M2H was lower than that of M2L.

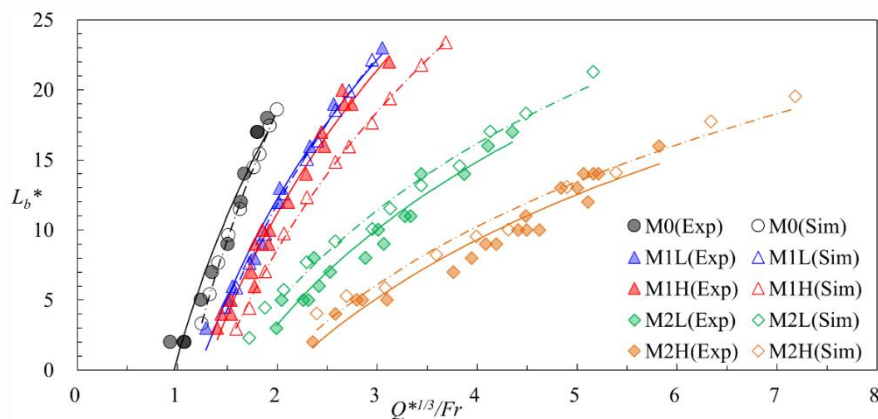


Figure 13. Comparison of the simulated and experimental results for the relationship between  $L_b^*$  and  $Q^{*1/3}/Fr$ .

4. The effect of Vehicle Blockage Ratio on Backlayering Characteristics

4.1. Li et al.'s Empirical Equation of Backlayering Length

According to the Froude similitude [16], we proposed the dimensionless value of the correlation  $Q^{*1/3}/Fr$  composed of the dimensionless backlayering length  $L_b^*$ , the convective heat release rate  $Q^*$ , and the longitudinal velocity  $U_m$ , presented as Equation (18).

$$L_b^* = \begin{cases} a \ln(b Q^{*1/3}/Fr), & Q^* \leq 0.15 \\ a \ln(c / Fr), & Q^* > 0.15 \end{cases} \tag{18}$$

Through fire experiments in a small-scale model tunnel, Li et al. (2010) set the value of  $a$  to 18.5, the value of  $b$  to 0.81, and the value of  $c$  to 0.43 without congested vehicles, and the value of  $a$  to 13.5, the value of  $b$  to 0.63, and the value of  $c$  with congested vehicles [13]. The value of  $c$  was set to 0.33. Additional remarks are given here, as this study used the cross-sectional area  $A$  of the tunnel as the parameter of the denominator for calculating  $Q^*$ , which, in this method, is slightly different from that of the study of Li et al. (2010), which

adopted the square of  $H$  as the parameter for calculating  $Q^*$  [16]. The relationship of the upper expression in Equation (18) is a straight line in Figure 14 with  $\ln(Q^{*1/3}/Fr)$  on the horizontal axis and  $L_b^*$  on the vertical axis, and  $a$  is the slope representing the backlayering length extension rate.

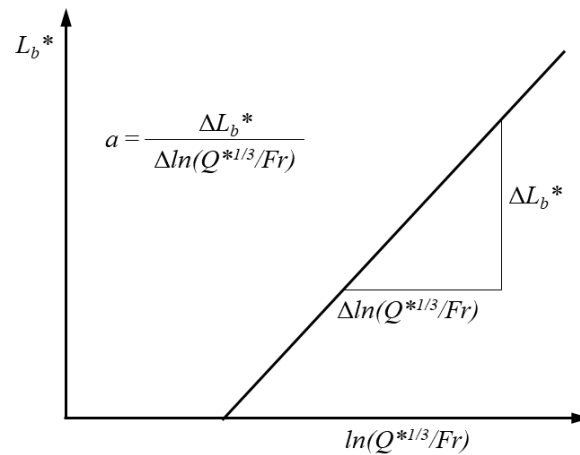


**Figure 14.** Linear relationship between  $\ln(Q^{*1/3}/Fr)$  and  $L_b^*$ .

Furthermore, when  $L_b^* = 0$  in the upper expression in Equation (18),  $Fr_{cr}$  becomes the dimensionless critical velocity preventing the backlayering, and the relation is as shown in Equation (19).

$$Fr_{cr} = b Q^{*1/3}, \quad Q^* \leq 0.15 \quad (19)$$

Since  $b$  corresponds to the critical velocity of backlayering prevention, it is expressed as the block backlayering characteristic. The value of  $c$  in Equation (20) is the super-critical velocity to prevent backlayering.

$$Fr_{scr} = c, \quad Q^* > 0.15 \quad (20)$$

When  $Q^* = 0.15$ , the upper and lower expressions in Equation (18) are the same.

$$c = 0.531b \quad (21)$$

As shown in Equation (21),  $c$  can also be obtained after the value of  $b$  has been obtained. Therefore, this study discusses  $a$  and  $b$  for  $Q^* < 0.15$ .

#### 4.2. Comparison and Discussion of Pattern A and Pattern B

Previous studies [15–19,22,28,29] also found that vehicular blockages cause a decrease in  $U_{cr}$  and that  $L_b$  becomes shorter. The positional relationship between the simulated fire source and the obstacle in this experiment was that the fire source was located in the central part of the tunnel section's width, the vehicles were located in a unilateral single lane or two lanes, and the obstacle was arranged without shielding the longitudinal airflow blown to the fire source (Figure 15a); this was Pattern A. The positional relationship of an obstacle shielding the fire source was also considered (Figure 15b); this was Pattern B. In this study, Pattern A was used for the experiments and simulations, while Pattern B was used only in the simulations.

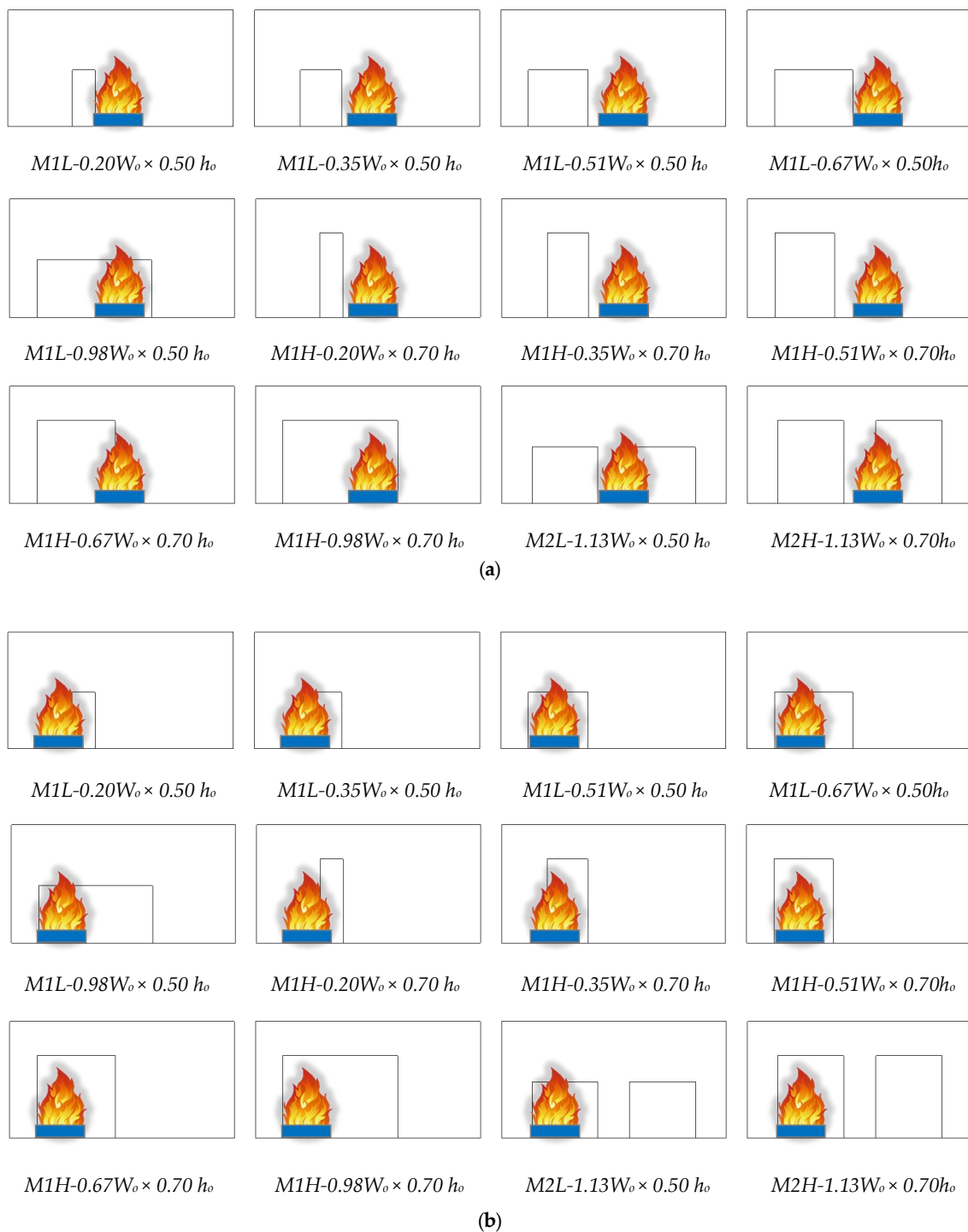


**Figure 15.** Configuration of fire sources and obstacles: (a) Pattern A; (b) Pattern B. (units: m).

In this study, the backlayering characteristics were divided into *a* and *b* to investigate the effects of the blockage ratio induced by the obstacle (the vehicle(s)). Figure 16 shows the effects induced by the vehicular blockage ratio *R* on the progression characteristic *a* of backlayering. The vertical axis is the ratio of *a* to *a*<sub>0</sub> (*a* when the blockage ratio is 0); the horizontal axis is the blockage ratio. The experiment (shown as navy-blue squares ■) started from the blockage ratio and proceeded according to the order of M1L, M1H, M2L, and M2H. The simulation results included M1L (medium-blue squares ■) and M1H (brown squares ■) with the same height and arrangement, only changing the width of the obstacle, and the results of M2L (yellow squares ■) and M2H (light-blue squares ■).

The solid line is the approximation formula, and the quadratic equation is  $a/a_0 = AR^2 + B$ . The primary terms were neglected, but the quadratic equation was selected, because if  $R$  increases, the progression of backlayering will be suppressed positively. Reducing  $a$  was considered. However,  $B$  was not set as 1, because if the obstacle vehicle width was reduced to approximately 0, it would still be a thin plate-like obstacle and may not have been coincident with the case without an obstacle. The resulting approximation formula of least squares is  $a/a_0 = -3.04R^2 + 0.889$ . Especially in the  $R < 0.2$  domain with a low blockage ratio, the experiment and simulation results coincide with each other. If  $R > 0.2$ , mild deviation can be found but with no large deviation. In the case of the semicircular tunnel section tunnel of Li et al. (2010) [16], because the fire source of this study was placed under the train, it was difficult to clearly classify it as Pattern A or Pattern B. Based on this consideration, this study used the experimental data of Li et al. (2010) [16] in both Pattern A and Pattern B. The experimental  $a_0 = 18.5$  when  $R = 0$ ,  $a$  was 13.5 when the blockage ratio was 20%, and  $a/a_0$  was 0.73. Thus, the result of the approximation formula approached 0.766, and thus the approximation formula of this study is applicable to different cross-sectional shapes.

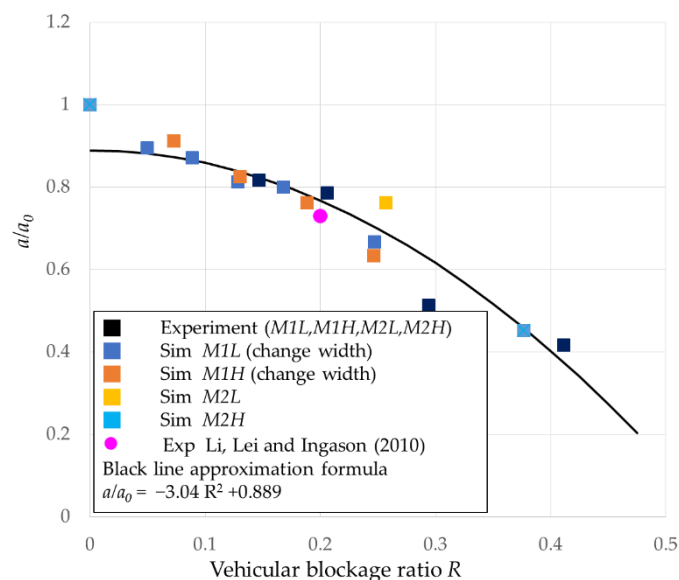


**Figure 16.** Approximation formula of  $a/a_0$  for Pattern A.

Figure 17 shows that the backlayering prevention characteristic  $b$  had a similar result. The same approximation formula was  $b/b_0 = -2.11R^2 + 0.922$ . While the experiment and the simulation were coincident with each other in the range of  $R < 0.2$ , slight deviation could be observed at  $R > 0.2$ . According to the results of Li et al. (2010) [16],  $b/b_0 = 0.78$  when  $R = 0.2$ . Although the  $b/b_0$  value was slightly lower than the approximation formula 0.842 of this study, it was approximately the same as the approximate value. In the case of a road tunnel, the cross-sectional shape was the determinant, but the cross-section area of a two-lane section was generally 45–70 m<sup>2</sup>, with the projected area of a large vehicle being 8–9 m<sup>2</sup> and the blockage ratio being 11–20%. Even if two large vehicles were side by side, the vehicular blockage ratio  $R$  was, at most, about 40%, so the vehicular blockage ratio  $R$  of one large vehicle was about 0.15–0.2.

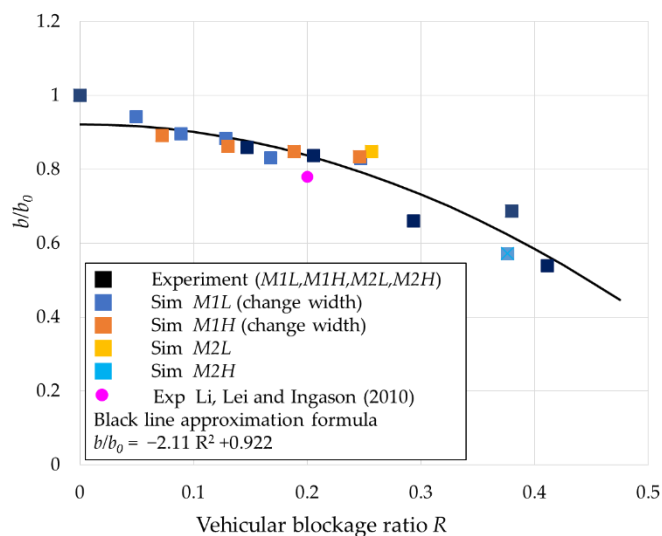


Figure 17. Approximation formula of  $b/b_0$  for Pattern A.

In Pattern B, the effect of the blockage ratio on the backlayering length extension rate  $a$  is shown in Figure 18a, and the effect of the blockage ratio on the block backlayering length characteristic  $b$  is shown in Figure 18b. The approximant derived from these results was  $a/a_0 = -4.68R^2 + 0.850$  and  $b/b_0 = -3.49R^2 + 1.06$ . If we compare the value of  $b$  in Pattern A in Figure 17 with the value of  $b$  in Pattern B in Figure 18b when  $R = 0.2$ , the  $b$  of Pattern A is smaller than the  $b$  of Pattern B. Since  $b$  is the block backlayering length characteristic and  $b$  is proportional to  $u_{cr}$ , this means that the  $u_{cr}$  of Pattern B is greater than that of Pattern A. The results of this part show the same trend as the results of Lee and Tsai (2012) [22], that is, the change in  $u_{cr}$  with vehicles depended on the relative position of the fire and vehicles.

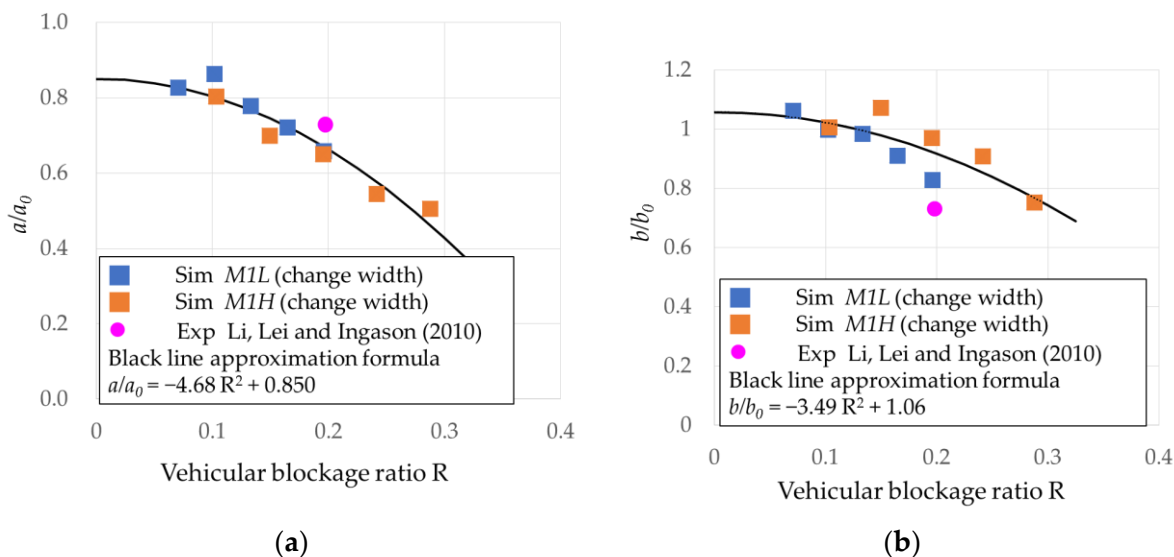


Figure 18. Approximation formula of Pattern B: (a)  $a/a_0$ ; (b)  $b/b_0$ .

### 4.3. Verification and Discussion of the Approximation Formula

The previous section focused on Pattern A, in which the longitudinal airflow in the  $x$ -direction blows directly to the fire source, and Pattern B, in which the obstacle blocks the longitudinal airflow in the  $x$ -direction. The approximation formula was obtained according to the vehicular blockage ratio  $R$  of the backlayering characteristics  $a$  and  $b$ . The prediction accuracy of the approximation formula was verified by changing the obstacle height and configuration in the previous section. The tunnel size and material were the same as in

the model tunnel of the experiment, namely 44.2 m in length, 1.93 m in width, and 1 m in height, and the wall and ceiling material was ALC slabs. The length of the obstacle in the  $x$ -direction and  $y$ -direction were set to the same value. The configuration is shown in Figure 15, with the obstacles in a unilateral single lane or two lanes. The  $x$ -direction distance from the fire source’s center to the front of obstacle was set as  $\ell_b$ , while the  $\ell_b$  of the unilateral single lane was changed across 1 m, 3 m, and 5 m. The value of  $\ell_b$  was 3 m in the case of two lanes, and the interval between each obstacle was 2 m in the  $x$ -direction. Figure 19 shows the fire source’s position for Pattern B. The position of the fire source for Pattern A and Pattern B is the center of the width,  $y = 0$  m. The simulated number of segmentations was identical to that of the simulation in Section 3, with  $D_x = 0.050$  m,  $D_y = 0.039$  m, and  $D_z = 0.032$  m. In the case of a single lane, there were four cases of obstacle height  $h_o$ , including  $h_o = 0.26$  m (8 cells), 0.39 m (12 cells), 0.58 m (18 cells), and 0.77 m (24 cells). In the case of two lanes, there were six cases, including the abovementioned four cases plus 0.48 m (15 cells) and 0.68 m (21 cells). The fire source was the model experiment’s fire source with an area of 0.15 m<sup>2</sup>. If the average heat release rate was 154 kW during complete combustion, the area was 0.13 m<sup>2</sup> with the  $x$ -direction being 0.3 m (6 cells) and the  $y$ -direction being 0.43 m (11 cells). Due to the cells’ dimension, a small fire source area was set. The dimensionless heat release rate  $Q^*$  was 0.037, the longitudinal velocity was set as  $U_m = 0.45$  m/s with the obstacle being set at  $x = 30$  m, and the Froude number was set to  $Fr = 0.14$  by controlling the backlayering length to up to 25 m.

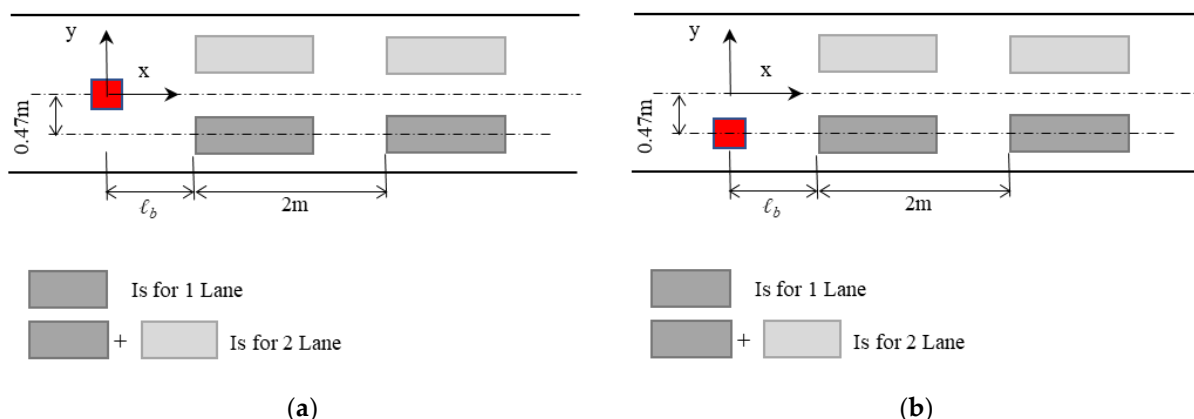
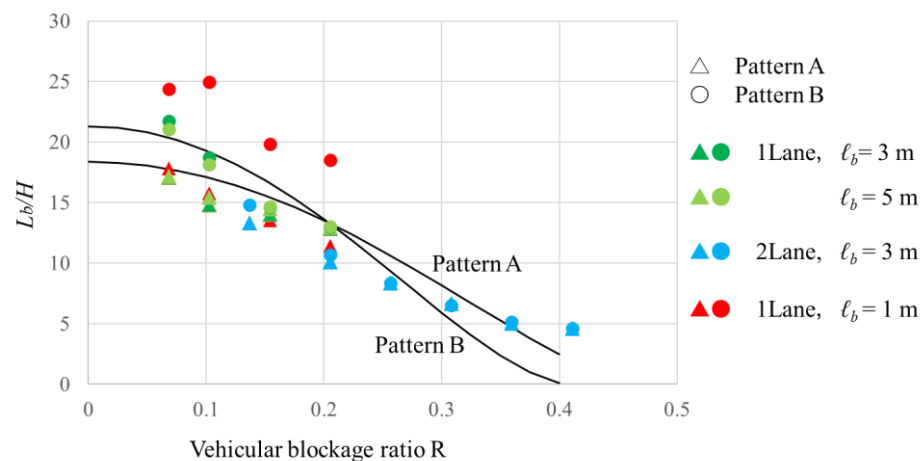


Figure 19. Top view of fire sources and obstacles: (a) Pattern A; (b) Pattern B.

Figure 20 shows the effect of the blockage ratio induced by the backlayering length when the height of obstacle was changed to 0.39 m and 0.65 m, and the distance from the fire source’s center to the front of the obstacle nearest to the fire source was changed to 1 m, 3 m, and 5 m. The figure describes the condition when the thermal velocity was  $Q_m = 77$  kW and the longitudinal velocity was  $U_m = 0.5$  m/s ( $Q^{*1/3}/Fr = 2.06$ ). In addition, in terms of the signs in the figure, Pattern A is marked as  $\Delta$  and Pattern B is marked as  $\circ$ . Blue indicates that the obstacles were placed side by side in two lanes; red shows that the  $\ell_b$  of a single lane was 1 m; dark green was used for  $\ell_b = 3$  m; light green was used for  $\ell_b = 5$  m. It can be observed in the figure that when the obstacles were placed side by side in two lanes, the difference between Pattern A and Pattern B was slight; when the blockage ratio was lower than 0.3, the backlayering length was lower than the approximation formula of Pattern A by 2.3 m, almost presenting a parallel migration to that in Pattern A. However, when the blockage ratio exceeded 0.3, there was a slight change in the backlayering length. According to our analysis, when the obstacle was 3 m away from the fire source, the smoke generated by the fire source was free from interference by the obstacle within 3 m; hence, it was likely to rise up. In Pattern A, with an obstacle only in a single lane,  $\ell_b$  showed slight differences between 1 m, 3 m, and 5 m, forming a backlayering length lower than that of the approximation formula of Pattern A by 1.2 m; however, it changed roughly in

line with the approximation formula of Pattern A. For Pattern B, which only considers a single lane, when  $\ell_b$  was 1 m (●), 3 m (●), and 5 m (●), there were large differences. In the case of 3 m and 5 m, the blockage ratio was 0.15, and a backlayering length 2 m lower than that of the approximation formula of Pattern B was applicable. When the blockage ratio was higher than 0.15, it could change in line with the approximation formula of Pattern B. Additionally, the approximation formulae of Pattern A and Pattern B were crossed with a blocking rate of 0.15. When the blockage ratio exceeded 0.15 (obstacles side by side limited to two lanes), the difference between Pattern A and Pattern B was small. When  $\ell_b$  was 1 m, the backlayering length was quite long, and the effect induced by the blockage ratio was not uniform or stable.



**Figure 20.** The effect of the vehicular blockage ratio on  $L_b/H$  in the case of Pattern A and Pattern B.

In order to investigate the reason for this, Figure 21 shows the distribution of the  $x$ -direction velocity  $-u/U_m$  when the blockage ratio was 0.2 and  $\ell_b$  was 1 m and 3 m. The upper figure shows the horizontal plane of  $z = 0.5$  m, and the lower figure shows the longitudinal section of  $y = -0.5$  m, penetrating through the center sections of the fire source and the obstacle. Regarding the longitudinal velocity from right to left, in the lane without the obstacle, the longitudinal velocity was 1.5–2 times the average longitudinal velocity  $U_m$ , but the front of the obstacle (left side) was the contraflow domain of the mainstream, within 1 m from the front of obstacle. If  $\ell_b = 3$  m, the longitudinal velocity in the fire source area was 0.8–1 times the average longitudinal velocity. However, if  $\ell_b = 1$  m, the fire plume was pulled to the obstacle through this reflux area, and the backlayering length was increased, creating instability.

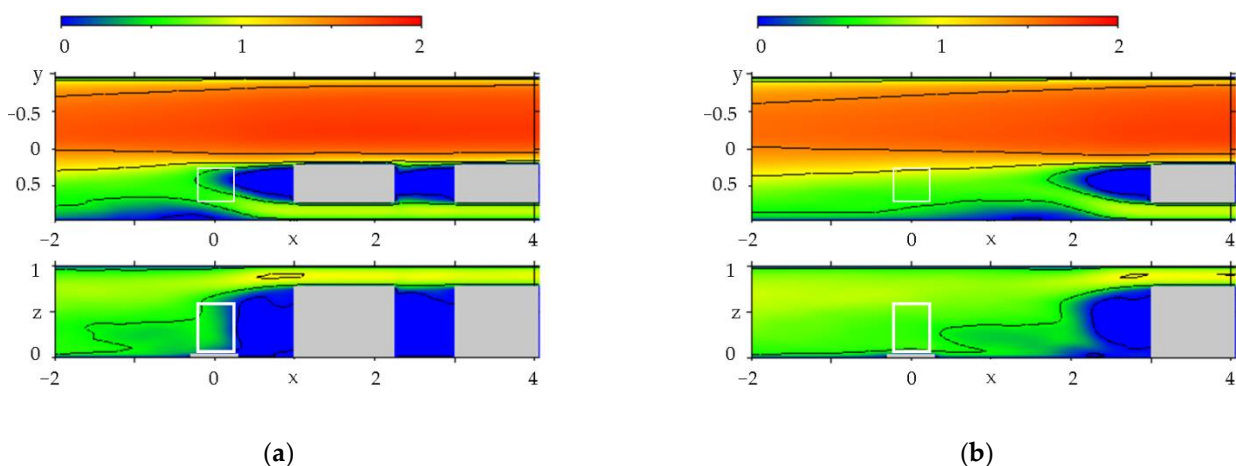


**Figure 21.** The distribution of the  $x$ -direction velocity  $-u/U_m$ ,  $R = 0.2$ : (a)  $\ell_b = 1$  m; (b)  $\ell_b = 3$  m.

According to this research, nearly all backlayering length with obstacles could be approximated by the approximation formula of Pattern A. If the blockage ratio was lower than 0.1 when a single lane had an obstacle, the approximation formula of Pattern B was applicable. However, when the fire source was close to the obstacle, the backlayering length was unstable and it could not be represented by the approximation formulae of this study.

## 5. Conclusions

If we compare the model experiment and the scale model simulation, the simulation can reproduce the backlayering thermal fumes created by the vehicle model. According to the comparison of the vehicle model configuration, the experimental results with changed heights, and the simulation results of the model tunnel, the simulator used in this study can predict the backlayering characteristics of thermal fumes accurately, even when the vehicle model's configuration and the height of the tunnel are changed. Specifically, this study investigated the effect of vehicular blockage on the backlayering length, with variables including the height and shape of the vehicular blockage, the configuration of the vehicular blockage, the vehicle blockage ratio, and whether the vehicular blockage blocked the longitudinal velocity, and finally presented some findings not obtained in previous studies, which are summarized as follows:

- According to the results, if there were vehicles on one side of Lane 1 (*M1L* and *M1H*), the height of the obstacle had little effect on the backlayering length extension rate  $a$ . Compared with the situation where there were vehicles on one side of Lane 1, when there were vehicles on both sides of the lane (*M2L* and *M2H*),  $a$  was significantly reduced. In addition, in the case of *M2H*,  $a$  had the greatest decrease. It was reduced to about 52% of  $a_0$  when there was no vehicle with a vehicle height of 2.62 m in *M2L* and to about 44% of  $a_0$  with a vehicle height of 3.57 m in *M2H*.
- In the configuration of Pattern A, when  $R < 0.2$  was in the low blocking rate domain, the experimental and simulated results were consistent. Even if  $R > 0.2$ , there was no significant deviation. In addition, the rectangular tunnel section used in this study was the same as the semicircular tunnel section used in previous studies. With the configuration of Pattern B, the approximation formulae were coincident with each other in the range of  $R < 0.2$ . Although slight deviation could be observed in  $R > 0.2$ , in reality, the vehicular blockage ratio  $R$  of one large vehicle was only about 0.15–0.2.
- Nearly all backlayering lengths with obstacles could be approximated by the approximation formula of Pattern A. If the blockage ratio was lower than 0.1 when a single lane had an obstacle, the approximation formula of Pattern B was applicable. However, when the fire source was close to the obstacle, the fire plume was pulled to the obstacle through this reflux region and the backlayering length became unstable, and it could not be represented by the approximation formula of this study.
- When the distance between stationary vehicles on the upstream side of the fire source was small, the backlayering length may have been longer than in the case with no vehicular blockage.

**Author Contributions:** Conceptualization, Y.-T.H.; software, N.K.; methodology, M.S.; formal analysis, M.H.; validation, N.K.; investigation, Y.-T.H.; resources, S.-W.C.; writing—original draft preparation, Y.-T.H.; writing—review and editing, N.K.; supervision, T.-S.S. All authors have read and agreed to the published version of the manuscript.

**Funding:** This research received no external funding.

**Institutional Review Board Statement:** Not applicable.

**Informed Consent Statement:** Not applicable.

**Data Availability Statement:** Not applicable.

**Acknowledgments:** We are grateful to Minehiro, T. and Yamamoto, Y. (ex-graduate student of Kanazawa University) for assistance with the experimental data. This work was supported by JSPS KAKENHI Grant Number JP16H03122.

**Conflicts of Interest:** The authors declare no conflict of interest.

## Nomenclature

$a$	Backlayering length expansion rate
$A_t$	Tunnel cross-section area (m <sup>2</sup> )
$A_v$	Vehicular cross-section area (m <sup>2</sup> )
$b$	Block backlayering length characteristic
$Bi$	Biot number: $Bi = hH/\lambda$
$Fo$	Fourier number: $Fo = \alpha(H/g)^{1/2}/H^2$
$Fr$	Froude number, $Fr = U_m / \sqrt{gH}$
$g$	Gravitational acceleration (m/s <sup>2</sup> )
$h$	Heat-transfer coefficient [W/(m <sup>2</sup> ·K)]
$H$	The height of the tunnel (m)
$HRR$	Heat release rate (kW)
$h_o$	The height of the obstacle (m)
$L_b$	Backlayering length of the thermal fume (m)
$L_b^*$	Dimensionless backlayering length $L_b^* = L_b/H$
$M0$	No vehicular blockage
$M1L$	One side with low vehicular blockage
$M1H$	One side with high vehicular blockage
$M2L$	Both sides with low vehicular blockage
$M2H$	Both sides with high vehicular blockage
$Q_m$	Average heat release rate (kW)
$Q^*$	Dimensionless average heat release rate $Q^* = Q_m / (\rho_0 C_p T_0 A \sqrt{gH})$
$R$	Vehicular blockage ratio ( $A_v/A_t$ )
$Re$	Reynolds number, $Re = U_m H/\nu$
$Ri$	Richardson number
$t$	Elapsed time after ignition (s)
$T_0$	Initial temperature (K)
$U_m$	Average ventilation longitudinal velocity in the cross-section (m/s)
$W$	The width of the tunnel (m)
$W_o$	The width of the obstacle (m)
$x$	Longitudinal axis of the tunnel
$y$	Transverse axis of the tunnel
$z$	Vertical axis ( $z = 0$ is the floor)
Pattern A	The fire source is located in the center of the tunnel
Pattern B	The fire source is on the side of the tunnel
Greek letters	
$\alpha$	Thermal diffusivity, $\alpha = \lambda/\rho C$ (m <sup>2</sup> /s)
$\lambda$	friction coefficient
$\nu$	Kinematic viscosity (m <sup>2</sup> /s)
$\rho_0$	Air density at ambient temperature (kg/m <sup>3</sup> )

## References

1. PIARC Fire and Smoke Control. In *PARIC Committee on Road Tunnels*; World Road Association, Committee on Intelligent Transport (C16): La Défense, France, 1999; ISBN 2-84060-064-1.
2. Fujita, K.; Minehiro, T.; Kawabata, N.; Tanaka, F. Temperature Characteristics of Backlayering Thermal Fume in a Tunnel Fire. *J. Fluid Sci. Technol.* **2012**, *7*, 275–289. [[CrossRef](#)]
3. Mizuno, A.; Ohashi, H.; Nakahori, I.; Okubo, N. Emergency operation of ventilation for the Kanetsu road tunnel. In *Proceedings of the 5th International Symposium on the Aerodynamics and Ventilation of Vehicle Tunnels*, Lille, France, 20 May 1985; pp. 77–91.
4. Mizuno, A. An optimal control with disturbance estimation for the emergency ventilation of a longitudinally ventilated road tunnel. In *Flucom 91, Proceedings of the 3rd Triennial International Symposium on Fluid Control, Measurement, and Visualization*, San Francisco, CA, USA, 1 June 1991; American Society of Mechanical Engineers: New York, NY, USA; pp. 393–399.

5. Mizuno, A.; Ichikawa, A. Controllability of longitudinal air flow in transversely ventilated tunnels with multiple ventilation divisions. In Proceedings of the First International Conference on Safety in Road and Rail Tunnels, Basel, Switzerland, 23 November 1992; pp. 425–437.
6. Vantelon, J.P.; Guelzim, A.; Quach, D.; Son, D.K. Investigation of Fire-Induced Smoke Movement in Tunnels and Stations: An Application to the Paris Metro. In Proceedings of the Third International Symposium on Fire Safety Science, Edinburgh, Scotland, 8 July 1991; pp. 907–918. [\[CrossRef\]](#)
7. Saito, N.; Sekizawa, A.; Yamada, T.; Yanai, E.; Watanabe, Y.; Miyazaki, S. Study Report on Fire Performance in Special Space of Use of Underground Space. *Fire Def. Res. Datum* **1994**, *29*.
8. Vauquelin, O.; Telle, D. Definition and Experimental Evaluation of the Smoke “Confinement Velocity” in Tunnel Fires. *Fire Saf. J.* **2005**, *40*, 320–330. [\[CrossRef\]](#)
9. Hu, L.; Peng, W.; Huo, R. Critical wind velocity for arresting upwind gas and smoke dispersion induced by near-wall fire in a road tunnel. *J. Hazard. Mater.* **2008**, *150*, 68–75. [\[CrossRef\]](#) [\[PubMed\]](#)
10. Minehiro, T.; Fujita, K.; Kawabata, N.; Hasegawa, M.; Tanaka, F. Backlayering Distance of Thermal Fumes in Tunnel Fire Experiments Using a Large-Scale Model. *J. Fluid Sci. Technol.* **2012**, *7*, 389–404. [\[CrossRef\]](#)
11. Tang, F.; Li, L.; Mei, F.; Dong, M. Thermal smoke back-layering flow length with ceiling extraction at upstream side of fire source in a longitudinally ventilated tunnel. *Appl. Therm. Eng.* **2016**, *106*, 125–130. [\[CrossRef\]](#)
12. Tanaka, F.; Takezawa, K.; Hashimoto, Y.; Moinuddin, K.A. Critical velocity and backlayering distance in tunnel fires with longitudinal ventilation taking thermal properties of wall materials into consideration. *Tunn. Undergr. Space Technol.* **2018**, *75*, 36–42. [\[CrossRef\]](#)
13. Zhang, T.; Wang, G.; Li, J.; Huang, Y.; Zhu, K.; Wu, K. Experimental Study of Back-layering Length and Critical Velocity in Longitudinally Ventilated Tunnel Fire with Various Rectangular Cross-sections. *Fire Saf. J.* **2021**, *126*, 103483. [\[CrossRef\]](#)
14. Kawabata, N.; Wang, Q.; Yagi, H.; Kawakita, M. Study of Ventilating Operation During Fire Accident in Road Tunnels with Large Cross Section. In Proceedings of the Fourth KSME-JSME Fluid Engineering Conference, Pusan, Korea, October 1998; pp. 53–56.
15. Kunikane, Y.; Kawabata, N.; Yamada, T.; Shimoda, A. Influence of Stationary Vehicles on Backlayering Characteristics of Fire Plume in a Large Cross Section Tunnel. *JSME Int. J. Ser. B* **2006**, *49*, 594–600. [\[CrossRef\]](#)
16. Li, Y.Z.; Lei, B.; Ingason, H. Study of critical velocity and backlayering length in longitudinally ventilated tunnel fires. *Fire Saf. J.* **2010**, *45*, 361–370. [\[CrossRef\]](#)
17. Tang, W.; Hu, L.; Chen, L. Effect of blockage-fire distance on buoyancy driven back-layering length and critical velocity in a tunnel: An experimental investigation and global correlations. *Appl. Therm. Eng.* **2013**, *60*, 7–14. [\[CrossRef\]](#)
18. Gannouni, S.; Ben Maad, R. Numerical study of the effect of blockage on critical velocity and backlayering length in longitudinally ventilated tunnel fires. *Tunn. Undergr. Space Technol.* **2015**, *48*, 147–155. [\[CrossRef\]](#)
19. Zhang, S.; Cheng, X.; Yao, Y.; Zhu, K.; Li, K.; Lu, S.; Zhang, R.; Zhang, H. An experimental investigation on blockage effect of metro train on the smoke back-layering in subway tunnel fires. *Appl. Therm. Eng.* **2016**, *99*, 214–223. [\[CrossRef\]](#)
20. Meng, N.; Liu, X.; Li, X.; Liu, B. Effect of blockage ratio on backlayering length of thermal smoke flow in a longitudinally ventilated tunnel. *Appl. Therm. Eng.* **2018**, *132*, 1–7. [\[CrossRef\]](#)
21. Meng, N.; Yang, W.; Xin, L.; Li, X.; Liu, B.; Jin, X. Experimental study on backlayering length of thermal smoke flow in a longitudinally ventilated tunnel with blockage at upstream of fire source. *Tunn. Undergr. Space Technol.* **2018**, *82*, 315–324. [\[CrossRef\]](#)
22. Lee, Y.-P.; Tsai, K.-C. Effect of vehicular blockage on critical ventilation velocity and tunnel fire behavior in longitudinally ventilated tunnels. *Fire Saf. J.* **2012**, *53*, 35–42. [\[CrossRef\]](#)
23. Ejiri, Y.; Kawabata, N.; Mori, F. Large eddy simulation of fire in transverse ventilation tunnels. In Proceedings of the Tunnel Fires-Fifth International Conference, Melbourne, Australia, 3–7 October 2004; pp. 121–130.
24. Tsai, K.-C.; Chen, H.-H.; Lee, S.-K. Critical ventilation velocity for multi-source tunnel fires. *J. Wind Eng. Ind. Aerodyn.* **2010**, *98*, 650–660. [\[CrossRef\]](#)
25. Kunikane, Y.; Kawabata, N.; Takekuni, K.; Shimoda, A. Heat Release Rate Induced by Gasoline Pool Fire in a Large-Cross-Section Tunnel. *Tunn. Manag. Int.* **2003**, *6*, 22–29.
26. Kawabata, N.; Kunikane, Y.; Yamamoto, N.; Takekuni, K.; Shimoda, A. Numerical Simulation of Smoke Descent in a Tunnel Fire Accident. *Tunn. Manag. Int.* **2003**, *6*, 357–366.
27. Jang, H.-M.; Chen, F. On the determination of the aerodynamic coefficients of highway tunnels. *J. Wind Eng. Ind. Aerodyn.* **2002**, *90*, 869–896. [\[CrossRef\]](#)
28. Oka, Y.; Atkinson, G.T. Control of smoke flow in tunnel fires. *Fire Saf. J.* **1995**, *25*, 305–322. [\[CrossRef\]](#)
29. Kang, K. Characteristic length scale of critical ventilation velocity in tunnel smoke control. *Tunn. Undergr. Space Technol.* **2010**, *25*, 205–211. [\[CrossRef\]](#)